ADVANCED FUNCTIONAL MATERIALS
www.afm-journal.de

High-Throughput Fabrication of Au–Cu Nanoparticle Libraries by Combinatorial Sputtering in Ionic Liquids

Dennis König, Kai Richter, Alexander Siegel, Anja-Verena Mudring, and Alfred Ludwig**

Materials libraries of binary alloy nanoparticles (NPs) are synthesized by combinatorial co-sputter deposition of Cu and Au into the ionic liquid (IL) 1-butyl-3-methylimidazolium bis(trifluoromethylsulfonyl)imide ([C_1C_4im][Tf_2N]), which is contained in a micromachined cavity array substrate. The resulting NPs and NP-suspensions are investigated by transmission electron microscopy (TEM), X-ray diffraction (XRD), UV-Vis measurements (UV-Vis), and attenuated total reflection Fourier transformed infrared (ATR-FTIR) spectroscopy. Whereas the NPs can be directly observed in the IL using TEM, for XRD measurements the NP concentration is too low to lead to satisfactory results. Thus, a new NP isolation process involving capping agents is developed which enables separation of NPs from the IL without changing their size, morphology, composition, and state of aggregation. The results of the NP characterization show that next to the unary Cu and Au NPs, both stoichiometric and non-stoichiometric Cu–Au NPs smaller than 7 nm can be readily obtained. Whereas the size and shape of the alloy NPs change with alloy composition, for a fixed composition the NPs have a small size distribution. The measured lattice constants of all capped NPs show unexpected increased values, which could be related to the NP/surfactant interactions.

1. Introduction

Metal nanoparticles (NPs) have found many applications, the most important possibly being in catalysis. Noble metal NPs such as Pd,[1] Pt,[2] Rh,[3] Ir,[4] or Ru[4] are efficient catalysts for hydrogenation reactions. Furthermore, nanoscale Au and Cu efficiently catalyze both methanol synthesis from CO[5,6] and the oxidation of alcohols[7] and CO.[8] While unary metal NPs are quite well explored, reports on alloy NPs are less, despite the fact that in alloys it is possible to tune the electronic properties and thus the chemical reactivity and catalytic activity for a given reaction. Examples are Pt–Cu and Pd–Cu alloy NPs which were used for the reduction of nitrates or Pt–Pd and Pt–Ni alloy NPs for the catalytic oxidation of methanol.[9–14] The tailored fabrication of binary and multinary alloy NPs for specific applications is still challenging. By using classical wet chemistry approaches, it is quite difficult to achieve a defined composition even for binary alloy NPs not to mention multinary.[15] Classical synthesis involves either the thermal decomposition or the reduction of a metal precursor, typically either a simple salt or an organometallic precursor molecule, for each metal that is involved in the final metal alloy. However, as the kinetic reaction rates for the reaction are different for each metal source due to their different reactivity, it is almost impossible to tune the final alloy composition over a wider range of stoichiometric ratios—especially when one metal is substantially nobler than the other, like Cu and Au. Additionally, wet chemical approaches lead to the formation of byproducts.

However, fabrication of alloy NPs with tunable composition is desired for many applications. Thus, for the fabrication of binary or multinary NPs new synthesis routes are strongly sought after. Albeit in recent years a number of synthesis routes for stoichiometric alloy NPs were developed, up to now a versatile synthetic procedure that allows manufacturing complete sets of well-comparable NPs with easily variable and well-defined composition in one experiment is still lacking.

As physical vapour depositions processes (like evaporation, sputtering, or laser ablation) do not rely on the different reactivity of starting materials, they appear to be the methods of choice for the manufacturing of alloy NPs with tailored compositions without chemical precursors or stabilizing agents.

In recent years, it was discovered that ionic liquids (ILs) are excellent media for the preparation and stabilization of NPs.[16–22] ILs are composed of large and complex ions and have an unusually low melting point. ILs which are liquid at room temperature (RT) are so called RTILs. They have received considerable attention as neoteric and tuneable solvents and reaction media. ILs offer the advantage that they are also able to

D. König, A. Siegel, Prof. A. Ludwig
Institute for Materials
Faculty of Mechanical Engineering
Ruhr-Universität Bochum, 44801, Bochum, Germany
E-mail: alfred.ludwig@rub.de
K. Richter, Prof. A.-V. Mudring
Inorganic Chemistry III
Faculty of Chemistry and Biochemistry
Ruhr-Universität Bochum, 44801, Bochum, Germany
E-mail: anja.mudring@rub.de
Prof. A.-V. Mudring
Materials Science and Engineering Department
Iowa State University
Ames, IA, 50011, USA
Prof. A.-V. Mudring, Prof. A. Ludwig
Materials Research Department
Ruhr-Universität Bochum
44801, Bochum, Germany

DOI: 10.1002/adfm.201303140

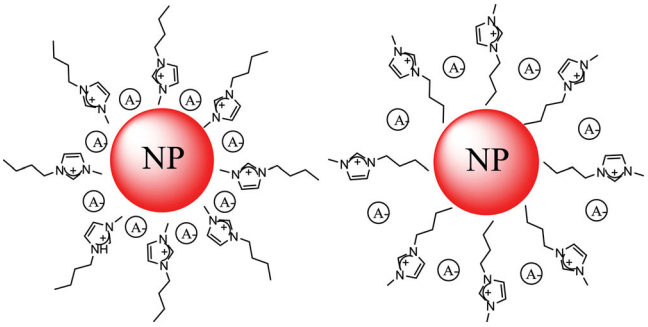

Figure 1. Examples for NP stabilization in ILs for surface charged, polar NPs (left) and for surface neutral, non-polar NPs (right).

act as the NP stabilizer and thus make the use of an additional surfactant unnecessary, reducing the number of chemicals employed even further. Consisting of cations and anions, ILs can form a protective electrostatic shell around NPs to prevent agglomeration. In addition, especially cations and anions with long or bulky alkyl chains may also sterically stabilize NPs in solution (**Figure 1**).

Laser ablation of a compound target in a liquid has been performed.[23] However, for each NP composition one special target is necessary. Thermal evaporation of transition metals into ILs was used by us to obtain long-time stable NP colloids, in this way also metal/metal–oxide composite materials were obtained.[24–26] Although this method is very powerful for unary NPs, the fabrication of binary or multinary NPs by evaporation into ILs is very challenging as it is difficult to control the evaporation ratios of metals with different vapour pressure.

The sputter technique is in such a case more adequate as it allows operating away from the thermodynamic equilibrium. For example thin films of binary, ternary or even quaternary composition can easily be fabricated by combinatorial magnetron sputtering from elemental targets. Furthermore, by fabricating ternary and large fractions of quaternary systems as materials libraries in one experiment on a single substrate,[27–29] sets of very well comparable samples are obtained. Moreover, a complete materials library assures that all desired compositions will be accessible for experiments. The Torimoto group pioneered the synthesis of metal NPs by sputtering in an IL.[30] It was observed that the NP size is strongly dependent on the IL,[31] where the viscosity of the IL has the greatest effect on the stability of the colloids. IL viscosity can be strongly affected by the IL water content [32] or temperature which impacts in the end the NP size.[33,34] Recently it was shown, that this sputter technique is not restricted to pure metals but could also be extended to binary noble metal alloy systems like Ag–Au.[35–37] Interestingly, it was claimed that Au–Pt alloy NPs were accessible by co-sputtering of Au and Pt into (*N,N,N*-trimethyl-*N*-propylammonium bis(trifluoromethylsulfonyl)amide, although in bulk, Au and Pt are immiscible.[38]

This finding motivated us to investigate the feasibility of the combinatorial fabrication of materials libraries of binary alloy NPs by sputter co-deposition into ILs. Our approach, visualized in **Figure 2**, allows a rapid screening of binary and multinary alloy NP systems.

2. Results and Discussion

2.1. Combinatorial Synthesis of Binary NPs in $[C_1C_4im][Tf_2N]$

Three materials libraries (ML) were fabricated, which are covering different compositional regions of the Au-Cu system: ML1 aimed on low Cu contents, ML2 aimed on low Au contents and ML3 aimed on compositions around $Au_{50}Cu_{50}$. ML4 was fabricated in order to prove the reproducibility of ML3. Furthermore, homogeneous depositions aiming for defined single NP compositions (pure Au, Cu, $Au_{92}Cu_8$, $Au_{75}Cu_{25}$, and $Au_{50}Cu_{50}$) were performed. These depositions were performed in order to obtain a larger amount of NPs with a specific chemical composition which enables characterization by other means than transmission electron microscopy (TEM) (e.g., X-ray diffraction (XRD) to determine the lattice parameters).

The compositions being present in the ML were characterized by high-throughput EDX. The EDX measurement results depicted in **Figure 3** show the composition ranges of the MLs measured on the thin films in between the cavities. All EDX measurements verify that the desired broad compositional region was achieved with one single deposition. The compositions of the NPs in the IL in the respective cavities were estimated by using the interpolated value of these measurements for the position of the cavity. In order to verify this, additional, nominally identical MLs were deposited under identical deposition conditions on non-structured Si/SiO_2 wafers, in order to measure the composition at these locations. The results (not shown here) prove the applicability of the interpolation. In the following it is assumed that the composition of the NPs in the cavities is the same as for the continuous thin film at this position. ML1 (black symbols) covers a compositional range from $Au_{15}Cu_{85}$ to $Au_{77}Cu_{23}$. ML 2 (red symbols) covers a compositional range from $Au_{41}Cu_{59}$ to $Au_{81}Cu_{19}$. For MLs 3 and 4 an almost identical compositional range was covered from $Au_{33}Cu_{67}$ to $Au_{80}Cu_{20}$. The error of the determined thin film compositions is about ±0.5 at.% for all EDX measurements.

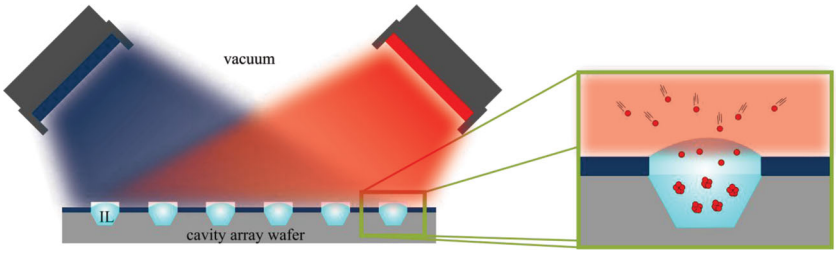

Figure 2. Left: schematic (not to scale) of the combinatorial co-deposition from two sputter targets into a cavity array substrate filled with IL. Right: Schematic of the proposed formation process of NP in IL.

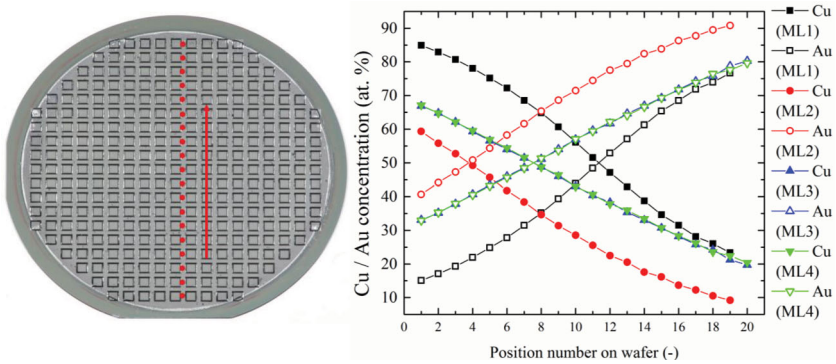

Figure 3. a) Photo of a 4-in cavity array substrate used for the fabrication of NP libraries. The red dots illustrate the measurement points whereas the red arrow illustrates the direction in which the EDX line scan analysis was performed. b) Results of EDX screening for the four materials libraries.

2.2. Characterization of NPs in IL

For the characterization of NPs in IL the elemental depositions of Au and Cu were analysed by TEM. **Figure 4** shows the TEM images and the particle size distributions of as-prepared Cu NPs measured directly in IL. The Cu-NPs dispersed in IL show a narrow size distribution with a NP size of 6.3 ± 0.9 nm. Similar sizes were obtained when thermally evaporating Cu into this IL.[17] It is experimentally quite demanding to investigate the NPs in the IL by TEM as the surrounding IL leads to a strong background signal. Therefore, we developed a new precipitation process (see below), to obtain stabilized NPs which can be transferred to other media without agglomeration and particle growth. This process leads to better observability of the NPs in the TEM since the contribution of the IL to the image is removed. After precipitation a NP diameter of 6.7 ± 0.8 nm was observed by TEM. This value coincides within error limits to the value observed for the NPs in IL.

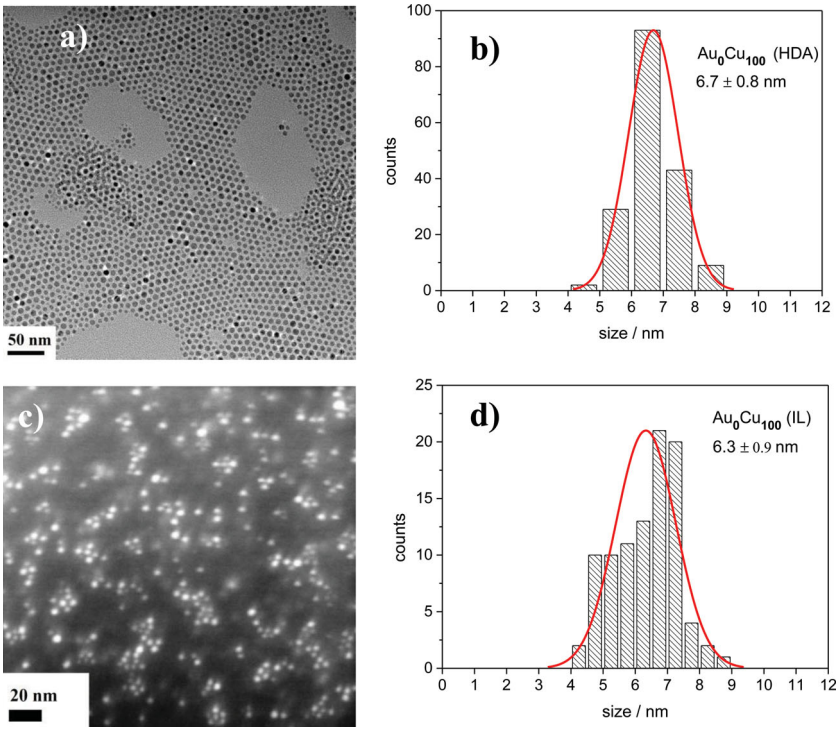

Figure 4. TEM images and size distributions of a,b) the HDA-capped Cu NPs and c,d) the as-prepared Cu NPs measured directly in IL without any capping agent. To enhance the contrast STEM-HAADF mode was used for image (c).

2.3. Precipitation Process

Janiak et al. reported that after direct addition of a capping agent, such as 1-dodecanthiole, fast precipitation of metal NPs from the IL was achieved. However an increase of the NP size was observed.[39] Therefore, a new protocol for the NP isolation was developed: Acetonitrile containing only a small amount of organic surfactants was added to the NP/IL colloid. As organic surfactants, acting as capping agents we used for the Cu NPs 1-hexadecylamine (HDA), and in the case of the Au NPs 1-dodecanethiol (DCT) and for all Au–Cu NPs a 1:1 mixture of HDA and DCT, respectively. After rinsing with pure acetonitrile alone no precipitation was observed. DCT and HDA interact strongly with the NP surface and were used as surfactants to stabilize Au und Cu NPs in classical synthesis methods.[40,41] The total concentration of the surfactants in acetonitrile was 0.02 wt% with respect to acetonitrile. Due to their long apolar alkyl chain, HDA and DCT themselves have a low solubility in acetonitrile and are virtually insoluble in the IL. Directly after the addition of the surfactant/acetonitrile mixture to the IL/NP/acetonitrile mixture a clear solution was observed. However, after a few days at room temperature the mixture becomes turbid and flocculation occurs. Then the precipitate was centrifuged and washed several times with acetonitrile and centrifuged again for 10 min at 2000 rpm. The collected, capped NPs can be easily redispersed in non-polar solvents, such as toluene. The capped Cu-NPs show a well-ordered arrangement on the TEM-grid and they have a constant interparticle-distance of around 3.8 nm (for TEM image see Supporting Information S1) due to the formation of a protection shell of HDA around the NP surface during the precipitation process. To investigate the surface interaction of the HDA with the Cu-NP surface attenuated total reflection Fourier transformed infrared (ATR-FTIR) spectroscopy was carried out. Figure S2 (Supporting Information) depicts the IR spectra of pure HDA in comparison with the precipitated and washed HDA-capped Cu NPs. In case of capped Cu-NPs the signals from the symmetric and asymmetric

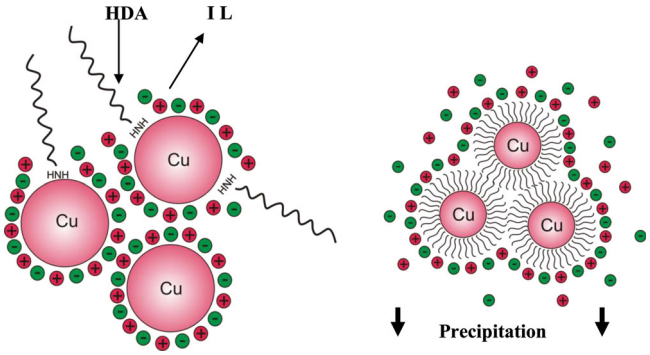

Figure 5. Postulated precipitation mechanism of the Cu NPs from the IL/acetonitrile mixture after adding of hexadecylamine.

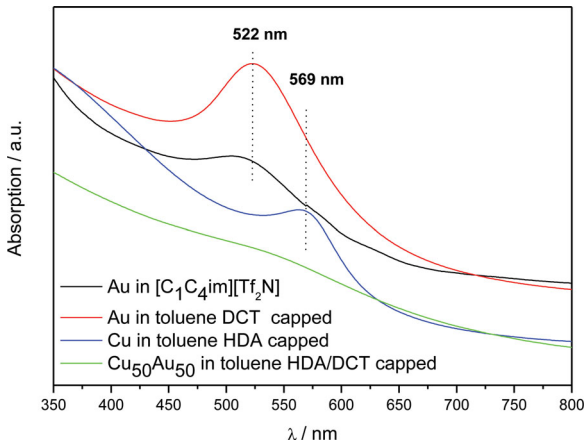

Figure 6. Absorption spectra of Cu, Au, and Au–Cu NPs.

stretching bond between hydrogen and nitrogen of the amine group at 3327 cm^{-1} and 3752 cm^{-1} disappear, as well as the signal attributed to the –NH deformation bending at 1610 cm^{-1}. The lack of the signals from the amino group of HDA is indicative of a strong interaction of the amine head group with the NP surface. As no signals from the IL were observed, a complete replacement of the IL against the capping agent can be assumed (for IR-spectra, see Supporting Information S2).

Based on these results the following precipitation mechanism is postulated (**Figure 5**): After adding HDA/acetonitrile, a slow replacement of the IL on the Cu-NP surface against the HDA occurs due to a stronger binding energy of the HDA to Cu. After forming a protection shell around the NPs, the apolar alkyl chains of the HDA interact by van-der-Waals forces with the ones from the neighbour-particle and form larger aggregates. The NPs are now protected. A low capping agent concentration and an excess of acetonitrile is the key to prevent NP agglomeration and growth. After formation of larger aggregates of capped NPs, the large apolar "outer" organic sphere leads to the precipitation out of the polar acetonitrile. These results show that this slow solvent/capping-agent precipitation method is useful to separate metal NPs from IL without significant change in size.

2.4. Characterization of Precipitated Au–Cu NPs

Based on the results with elemental NPs, precipitation experiments were carried out with the Au–Cu alloy NPs. **Figure 6** displays the absorption curves of the precipitated NPs redispersed in toluene (see also **Table 1**). Pure Au NPs dispersed in IL show a broad, less intense absorption maximum around 522 nm, compared to DCT-capped Au NPs. The lower intensity of the absorption can be attributed to the small concentration of NPs in IL and a suppression of the plasmon resonance by dipole-interaction of the surrounding IL. However, re-dispersed DCT-capped Au NPs show an absorption maximum at 522 nm with no significant shift in the absorption maximum. Generally, Au NPs show a shift of the plasmon resonance to higher wavelengths with increasing NP size.[25] Here, no shift is observed due to a constant NP size before and after the separation process. HDA-capped Cu NPs show an absorption maximum at 569 nm. In case of $Au_{50}Cu_{50}$ DCT/HDA-capped NPs, which were re-dispersed in toluene, no significant absorption maximum is observed.

2.5. Morphology and Size Distribution of Au–Cu NPs

TEM investigations were carried out in order to characterize the size and shape as well as the size distribution of the Au–Cu NPs, which were investigated in the DCT/HDA-capped state. **Figure 7** depicts TEM bright-field images of pure Au and Cu NPs and Au–Cu alloy NPs with different chemical compositions. Obviously, all NPs have different sizes with an average diameter < 7 nm. Some of them exhibit a non-spherical shape. For pure Cu NPs (Figure 7a) a mean diameter of 6.7 nm was determined. The Cu NPs are not agglomerated and show a uniform shape and size distribution. For pure Au NPs (Figure 7b) the shape is also spherical but the size of the NPs is not as uniform as for the Cu NPs. For Au NPs a mean diameter of 2.8 nm was determined. However, for Au–Cu NPs the spherical shape changes towards irregularly shaped NPs with increasing Cu content. **Figure 8** depicts particle size distributions of capped Au–Cu NPs with different compositions. The size of the NPs reduces with increasing Cu content up to a Cu concentration of 25 at%. For higher Cu contents the size of the NPs increases again. **Figure 9** depicts the NP size as a function of the Cu content. The NP size appears minimal for $Au_{75}Cu_{25}$ NPs. $Au_{92}Cu_8$ NPs are no longer spherical but have a more irregular angular shape (see Figure 7c). This trend is continued for compositions of $Au_{75}Cu_{25}$ and $Au_{50}Cu_{50}$. The mean NP diameter ranges from 2.7 ± 0.5 nm for $Au_{92}Cu_8$ over 2.0 ± 0.5 nm for $Au_{75}Cu_{25}$ to 2.5 ± 0.7 nm for $Au_{50}Cu_{50}$ (see Figure 8).

Table 1. Absorption maxima of Cu, Au and Au-Cu NPs.

NP composition	Solvent	Capping agent	Absorption maximum [nm]
Au	toluene	DCT	520
Au	$[C_1C_4im][Tf_2N]$	–	522
Cu	toluene	HDA	569
$Au_{50}Cu_{50}$	toluene	HDA/DCT	575 (weak)

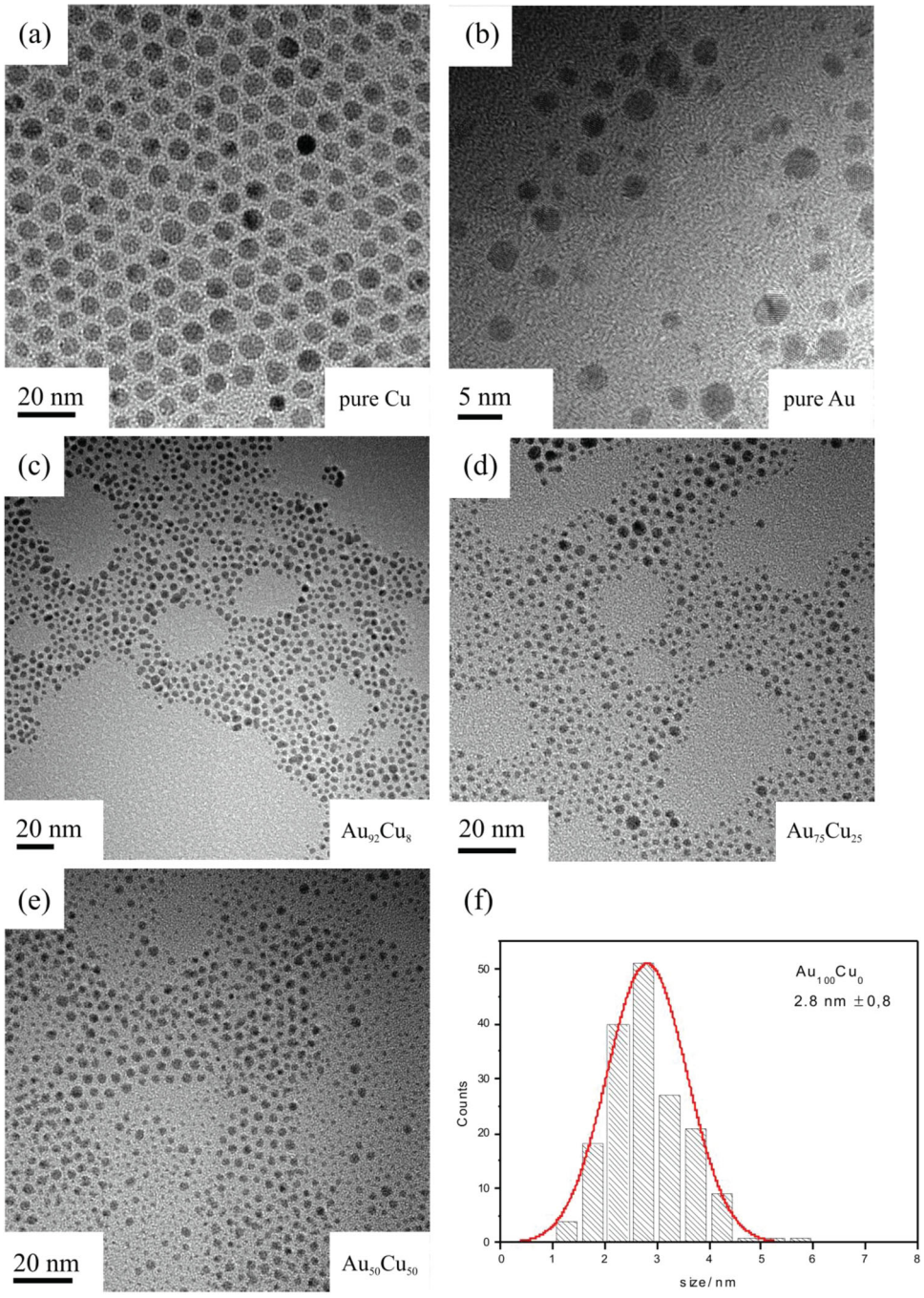

Figure 7. a,b) TEM bright-field images of elemental NPs as well as of c–e) Au–Cu alloy NPs with different chemical compositions. All were precipitated and capped with organic surfactants. Size and shape of the NPs change with changing composition. A representative NP size distribution is shown in (f). The red line in (f) represents a fit to the data.

2.6. Structural Analysis and Capping Effects

Figure 10a depicts XRD patterns in the angular range between $2\Theta = 35°$ and $2\Theta = 50°$ for capped NPs of Au, $Au_{92}Cu_8$, $Au_{75}Cu_{25}$, and $Au_{50}Cu_{50}$, collected from whole cavity array wafers. The diffraction angles for bulk Au are indicated by dashed lines. For Au NPs two peaks from the $(111)_{Au}$ and $(200)_{Au}$ planes are observed. The diffraction angles of the NPs coincide well with the diffraction angles for bulk Au. This result is surprising and will be explained below. For $Au_{92}Cu_8$ NPs, a slight shift of the diffraction peaks was observed, indicating a decrease of the lattice spacing caused by the substitution of smaller Cu into the Au lattice. Furthermore, the intensity of the (200) peak decreases. For $Au_{75}Cu_{25}$, the (111) peak shifts

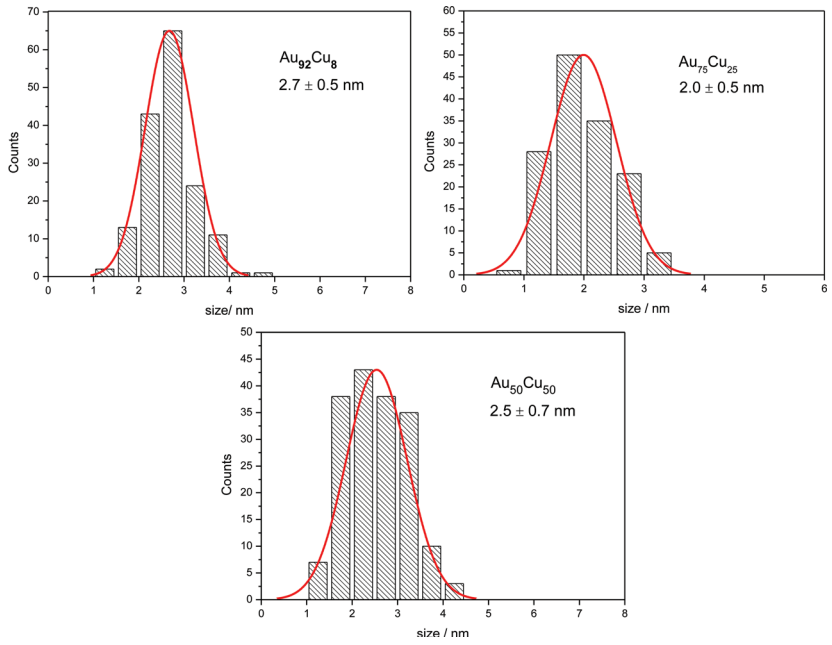

Figure 8. Particle size distributions of capped Au–Cu NPs with different compositions.

further to higher diffraction angles whereas the (200) peaks can only be observed as a shoulder of the (111) peak. For $Au_{50}Cu_{50}$ NPs this trend is continued.

From these diffraction patterns the lattice constants were determined by peak fitting using a Lorentz type function. Figure 10b depicts the determined lattice constants, in comparison to lattice constants of the corresponding bulk materials. Interestingly, all determined lattice constants are higher or the same (for pure Au) than the literature reference values for bulk materials. This is unexpected since the lattice constants for NPs are typically smaller than their bulk counterparts, due to lattice compression caused by the surface energy.[43,44] However, it is possible to calculate the lattice expansion of the capped NPs. Figure 10c depicts the lattice expansion with respect to the bulk values as a function of the Cu content. It is obvious that the lattice expansion increases almost linearly with increasing Cu content. This can be explained as follows: With increasing Cu content the fraction of Cu atoms at the NP´s surface increases and thus the number of coordinated hexadecylamine (HDA) capping molecules. However, when the number of these molecules at the surface increases the interaction between them becomes stronger. Therefore, we suggest that the observed lattice increase in all NPs is due to the increasing number of HDA molecules showing repulsive interaction amongst each other and thus increasing the lattice parameter. This explanation is supported by the decreasing grain size with increasing Cu content (see blue graph in Figure 10c). Since the atomic radius of Cu is significantly smaller than the atomic radius of Au the NPs become smaller with increasing Cu content. This results in a stronger constraint by the HDA molecules because the NP wants to contract but is hindered by the HDA molecules.

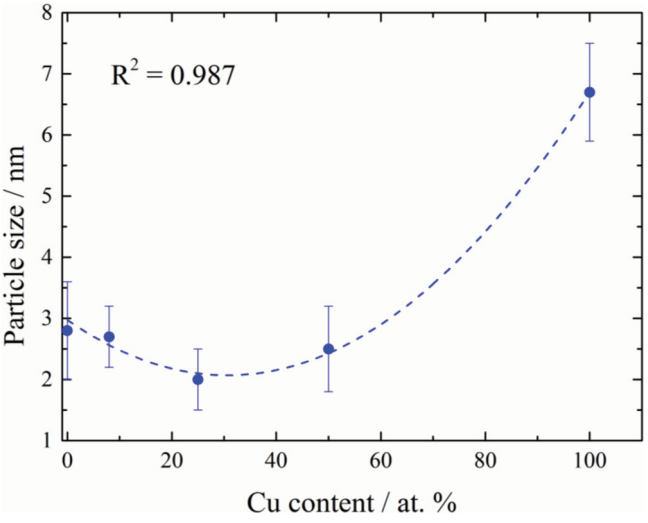

Figure 9. NP size as a function of Cu content in capped Au–Cu.

3. Conclusion

A binary library of alloy nanoparticles was fabricated by combinatorial sputtering into ionic liquids which are contained in a cavity array wafer. The NPs are small (<7 nm) and have a narrow size distribution, especially the elemental particles. The size and shape of the NPs change with composition. A precipitation protocol was developed which allows isolating the particles from the IL yet avoids agglomeration and any significant growth of NPs. The lattice constants of the isolated particles, as determined by XRD, showed increased values compared to the bulk, which can be explained by NP/surfactant interactions. The results show that this new high-throughput approach for the synthesis of complete libraries of NPs is feasible. The method is currently extended to multinary systems. A further development will be the transfer of the NP/IL library to other, linked high-throughput experiments such as loading a support material with the different NPs for combinatorial catalysis. This could be achieved by pipetting robots or by design of a microfluidic system. By that the combinatorial methodology could be extended from a level of materials screening to a systems screening level.

4. Experimental Section

Ionic Liquids: The IL 1-butyl-3-methylimidazolium bis(trifluoromethylsulfonyl)imide $[C_1C_4im][Tf_2N]$ (IoLiTec, Denzlingen, Germany) was dried at 80 °C under vacuum for 24 h in order to remove volatile impurities and water prior to use. The residual water content was

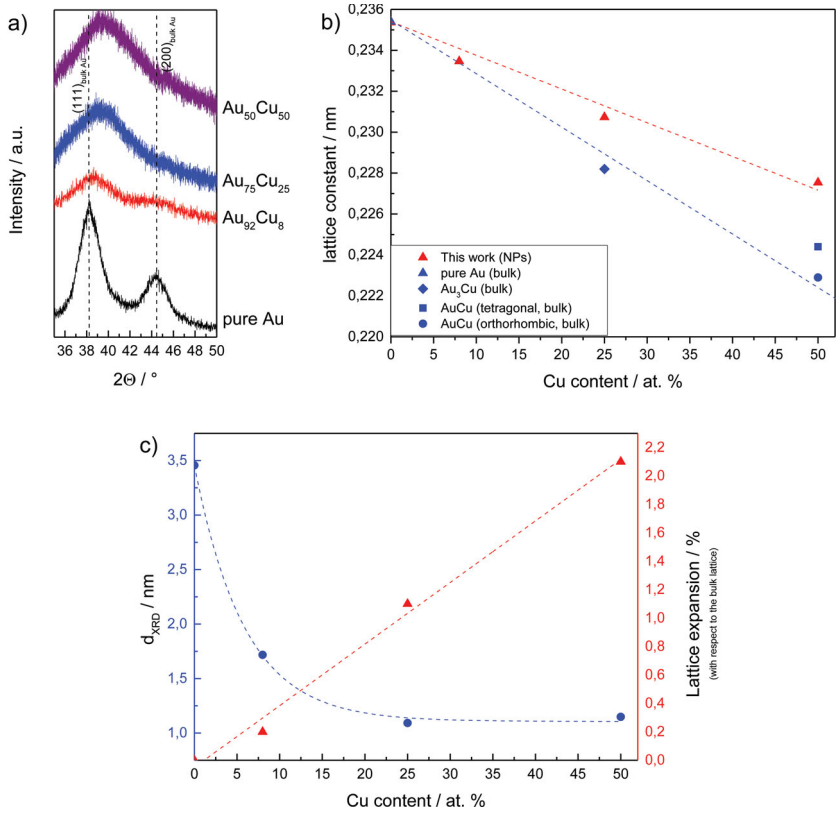

Figure 10. a) XRD diffraction patterns for precipitated and dried Au, $Au_{92}Cu_8$, $Au_{75}Cu_{25}$, and $Au_{50}Cu_{50}$ NPs. The dashed lines indicate the diffracting angles for bulk Au. b) Lattice constants determined in this work in comparison to lattice constants reported for bulk material in literature.[42] Dashed lines are guides for the eye. c) Grain size d_{XRD} (blue) and lattice expansion (red) as a function of the Cu content; d_{XRD} was determined using the Scherrer equation. The lattice expansion is plotted with respect to the values of the bulk lattice. Dashed lines are fits to the data and serve as guide for the eye.

Table 2. Sputter parameters for the elemental deposition, homogeneous alloy depositions and nanoparticle library depositions: the Ar partial pressure for all depositions was 5 mTorr at an Ar flow of 40 sccm.

Composition	Deposition power [W]	DC/RF	Deposition rate [nm s^{-1}]
Au	150	DC	0.42
Cu	168	RF	0.38
ML1	Au: 195	Au: DC	Au: 0.55
	Cu: 222	Cu: RF	Cu: 0.19
ML2	Au: 40	Au: DC	Au: 0.11
	Cu: 418	Cu: RF	Cu: 0.36
ML3/4	Au: 94	Au: DC	Au: 0.26
	Cu: 332	Cu: RF	Cu: 0.29
$Au_{92}Cu_8$ (homogen.)	Au: 143	Au: DC	Au: 0.40
	Cu: 73	Cu: RF	Cu: 0.06
$Au_{75}Cu_{25}$(homogen.)	Au: 195	Au: DC	Au: 0.55
	Cu: 222	Cu: RF	Cu: 0.19
$Au_{50}Cu_{50}$(homogen.)	Au: 98	Au: DC	Au: 0.27
	Cu: 311	Cu: RF	Cu: 0.27

determined by coulometric Karl-Fischer titration and was below 50 parts per million.

The capping agent hexadecylamine (HDA), purchased in technical grade from ABCR (Karlsruhe, Germany) was purified by recrystallization from hexane and the purity was confirmed by NMR-Spectroscopy. 1-dodecanthiole (DOT) (98% purity) was also obtained from ABCR, and used without prior purification.

Combinatorial Sputter Deposition: The combinatorial fabrication of alloy NPs materials libraries with a wide composition range was performed by co-sputtering from two elemental targets (Cu and Au, purity 99.995 at% and 99.99 at%, respectively) positioned opposite to each other. The inclination angle of 28° of the target with respect to the substrate normal (see Figure 2) leads to an approximately linear compositional gradient on the substrate, where the higher content of one material is achieved at the substrate position closer to the target. Co-sputtering was conducted under a pressure of 5 mTorr and under a constant Ar gas flow of 40 sccm. The sputter powers and rates are given in **Table 2**. For the realization of materials libraries of sputtered NPs in ILs a special substrate was designed, prepared and used. It consists of an array of 301 square cavities (lateral dimensions: 3 mm × 3 mm) with a depth of ≈300 µm etched in a 4-in (100)-oriented Si wafer (1.5 µm thermal SiO_2), which was structured by means of etching with buffered HF (RT) and KOH (30%, 80 °C) solutions. The cavities are regularly distributed across the wafer (4.5 mm apart from each other in all directions). The fabrication process is displayed schematically in **Figure 11**. Prior to the deposition of the materials libraries each of the cavities was filled with 2 µL of 1-butyl-3-methylimidazolium bis(trifluoromethylsulfonyl)imide by pipetting with an Eppendorf pipette, thereby assuring equal amounts of IL in each cavity. If large amounts of NPs of a certain composition were needed (e.g., for XRD) the whole cavity array substrate was coated homogenously. This was achieved by rotating the substrate with 20 rpm during co-deposition.

Isolation of the As-Prepared NPs: After deposition of a NP library, the 301 cavities filled with IL and loaded with different NP compositions by co-sputtering were emptied by pipetting. NP loaded ILs were either directly used for characterization or further processed. After the homogenous deposition, the NPs were rinsed off the whole cavity array

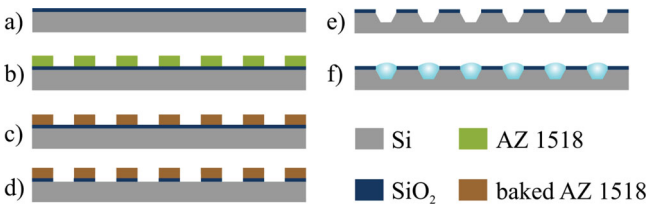

Figure 11. Fabrication process for cavity array substrates: a) 4-in (100)-oriented Si wafer with 1.5 µm SiO_2 on top serving as masking layer for the following KOH etch step. After cleaning the wafer with acetone and iPrOH, photoresist (AZ1518) is spun on and patterned (b). The photoresist is baked out (c) in order to increase its resistance against etching. (d) The baked photoresist is used as etch mask during local removal of the SiO_2 layer using buffered HF. After etching SiO_2, the photoresist is removed and the patterned SiO_2 serves as etch mask during KOH wet etching (e). For the fabrication of NPs in IL each cavity is filled with IL (f).

wafer with acetonitrile. The IL dissolves completely in acetonitrile and the NPs form, together with the solvent/IL-mixture, a stable colloid for months. Subsequently, a certain amount of 1-hexadecylamin (HDA) and/or 1-dodecanthiol (DCT), depending on the NP composition, is added in order to stabilize the NPs. For TEM investigations, this solution is dripped on commercial Cu grids coated with amorphous carbon (Plano, Wetzlar, Germany).

For XRD investigations, a complete cavity array wafer filled with IL is coated homogenously with a selected composition (i.e., fixed composition) in order to synthesize a larger amount of NPs. The film thickness equivalent of these depositions was 500 nm. After deposition into IL the NPs were precipitated using the process described above. Subsequently, the solvent was evaporated and the NPs were dried. XRD analysis was performed using a Panalytical MRD diffractometer (45 kV, 40 mA, Cu K_α radiation) equipped with a PiXcel line detector.

The elemental distribution over the materials library was determined by energy dispersive X-ray spectroscopy (EDX) analysis. This analysis was performed in the area between the cavities using a JEOL JSM 5800 LV scanning electron microscope (SEM) equipped with an Oxford INCA EDX system (20 kV, 10 mm working distance, 30 s per measurement).

FT-IR spectroscopy was carried out using a Bruker OPUS FT-IR (ATR) spectrometer with diamond reflection unit. The scan range was between 350 cm^{-1} to 3500 cm^{-1} with a resolution of 2 cm^{-1}. To perform the measurement a small amount of the colloid was dropped onto the diamond crystal and 10 scans were averaged.

For UV-Vis spectroscopy, a double-beam spectrometer Cary5000 from Varian (Agilent, Darmstadt) was used. The colloids were measured in cuvettes consisting of optical grade glass with 1 mm pathway from Helma between 200 and 800 nm wavelengths and a scan rate of 600 nm per minute. The resolution was 1 nm. To prevent oxidation of the colloids samples were prepared under inert atmosphere.

Received: September 9, 2013
Revised: October 16, 2013
Published online: December 2, 2013

[1] O. Trapp, S. K. Weber, S. Bauch, T. Baecker, W. Hofstadt, B. Spliethoff, *Chem. Eur. J.* **2008**, *14*, 4657–4666.
[2] C. W. Scheeren, G. Machado, J. Dupont, P. F. P. Fichtner, S. R. Texeira, *Inorg. Chem.* **2003**, *42*, 4738–4742.
[3] X.-D. Mu, J.-Q. Meng, Z.-C. Li, Y. Kou, *J. Am. Chem. Soc.* **2005**, *127*, 9694–9695.
[4] G. S. Fonseca, E. T. Silveira, M. A. Geleky, J. Dupont, *Adv. Synth. Catal.* **2005**, *347*, 847–853.
[5] S. Vokojevic, O. Trapp, J.-D. Grunwaldt, C. Kiener, F. Schueth, *Angew. Chem. Int. Ed.* **2005**, *44*, 7978–7981.
[6] T. Ressler, B. L. Kniep, I. Kasatkin, R. Schloegel, *Angew. Chem. Int. Ed.* **2005**, *44*, 4704–4707.
[7] J. Han, Y. Liu, R. Guo, *Adv. Funct. Mater.* **2009**, *19*, 1112–1117.
[8] S. Carretin, Y. Hao, V. Aguilar-Guerrero, B. C. Gates, S. Trasobares, J. J. Calvino, A. Corma, *Chem. Eur. J.* **2007**, *13*, 7771–7779.
[9] Z. Sun, J. Masa, W. Xia, D. König, A. Ludwig, Z.-A. Li, M. Farle, W. Schuhmann, M. Muhler, *ACS Catal.* **2012**, *2*, 1647–1653.
[10] S. Sarina, H. Zhu, E. Jaateinen, Q. Xiao, H. Liu, J. Jia, C. Chen, J. Zhao, *J. Am. Chem. Soc.* **2013**, *135*, 5793–5801.
[11] Y.-W. Lee, A.-R. Ko, S.-B. Han, H. S. Kim, K.-W. Park, *Phys. Chem. Chem. Phys.* **2011**, *13*, 5569–5572.
[12] S. Zhang, Ö. Metin, D. Su, S. Sun, *Angew. Chem. Int. Ed.* **2013**, *52*, 3681–3684.
[13] X.-J. Liu, C.-H. Cui, M. Gong, H.-H. Li, Y. Xue, F.-J. Fan, S.-H. Yu, *Chem. Commun.* **2013**, *49*, 8704–8706.
[14] N. Barrabés, J. Just, A. Davinov, F. Medina, J. L. G. Fierro, J. E. Sueiras, P. Salagre, Y. Casteros, *Appl. Catal. B: Environ.* **2006**, *62*, 77–85.
[15] I. S. Helgadottir, P. P. Arquillière, P. Bréa, C. C. Santini, P.-H. Haumesser, K. Richter, A.-V. Mudring, M. Aouine, *Microelectron. Eng.* **2013**, *107*, 229–232
[16] J. Dupont, G. S. Fonseca, A. P. Umpierre, P. F. P. Fichtner, S. R. Teixeira, *J. Am. Chem. Soc.* **2002**, *124*, 4228–4229.
[17] J. Huang, T. Jiang, H. X. Gao, B. X. Han, Z. Liu, W. Z. Wu, Y. H. Chang, G. Y. Zhao, *Angew. Chem. Int. Ed.* **2004**, *43*, 1397–1399.
[18] M. Antonietti, D. Kuang, B. Smarsly, Y. Zhou, *Angew. Chem. Int. Ed.* **2004**, *43*, 4988–4992.
[19] Z. Liu, B. X. Han, J. Huang, Z. Y. Zhang, T. Jiang, *Angew. Chem. Int. Ed* **2006**, *45*, 266–269.
[20] Y. Zhou, *Curr. Nanosc.* **2005**, *1*, 33–40.
[21] A.-V. Mudring, T. Alammar, T. Baecker, K. Richter, *ACS Symp. Series* **2009**, *1030*, 177–188.
[22] D. S. Jacob, L. Bitton, J. Grinblat, I. Felner, Y. Koltypin, A. Gedanken, *Chem. Mater.* **2006**, *18*, 3162–3168.
[23] J. Jakobi, A. Manjon, V. S. K. Chakravadhanula, L. Kienle, P. Wagener, S. Barcikowski, *Nanotechnology* **2011**, *22*, 145601.
[24] K. Richter, A. Birkner, A.-V. Mudring, *Angew. Chem. Int. Ed.* **2010**, *49*, 2431–2435.
[25] K. Richter, A. Birkner, A.-V. Mudring, *Phys. Chem. Chem. Phys.* **2011**, *13*, 7136–7141.
[26] K. Richter, P. S. Campbell, T. Bäcker, A. Schimitzek, D. Yaprak, A.-V. Mudring, *Phys. Status Solidi B* **2013**, *250*, 1152–1164.
[27] A. Ludwig, J. Cao, B. Dam, R. Gremaud, *Appl. Surf. Sci.* **2007**, *254*, 682–686.
[28] P. J. S. Buenconsejo, R. Zarnetta, D. König, A. Savan, S. Thienhaus, A. Ludwig, *Adv. Funct. Mater.* **2011**, *21*, 113–118.
[29] D. König, R. Zarnetta, A. Savan, H. Brunken, A. Ludwig, *Acta Mater.* **2011**, *59*, 3267–3275.
[30] T. Torimoto, K. Okazaki, T. Kiyama, K. Hirahara, N. Tanaka, S. Kuwabata, *Appl. Phys. Lett.* **2006**, *89*, 243117/1–243117/3.
[31] Y. Hatakeyama, M. Okamoto, T. Torimoto, S. Kuwabata, K. Nishikawa, *J. Phys. Chem. C* **2009**, *113*, 3917–3922.
[32] E. vert Vanecht, K. Binnemans, S. Patskovsky, M. Meunier, J. Won Seo, J L. Stappers, J. Fransaer, *Phys. Chem. Chem. Phys.* **2012**,*14*, 5662–5671.
[33] Y. Hatakeyama, K. Onishi, K. Nishikawa, *RSC Adv.* **2011**, *1*, 1815–1821.
[34] Y. Hatakeyama, S. Takahashi, K. Nishikawa, *J. Phys. Chem. C* **2010**, *114*, 11098–11102.
[35] T. Suzuki, K. Okazaki, T. Kiyama, S. Kuwabata, T. Torimoto, *Electrochemistry* **2009**, *77*, 636.
[36] K. Okazaki, T. Kiyama, K. Hirahara, N. Tanaka, S. Kuwabata, T. Torimoto, *Chem. Commun.* **2008**, 691–693.
[37] M. Hirano, K. Enokida, K. Okazaki, S. Kuwabata, H. Yoshidaa, T. Torimoto, *Phys. Chem. Chem. Phys.* **2013**,*15*, 7286–7294.
[38] S. Suzuki, T. Suzuki, Y. Tomita, M. Hirano, K. Okazaki, S. Kuwabata, T. Torimoto, *CrystEngComm* **2012**, *14*, 4922.
[39] E. Redel, M. Walter, R. Thomann, C. Vollmer, L. Hussein, H. Scherer, M. Krüger, C. Janiak, *Chem. Eur. J.* **2009**, *15*, 10047–10059.
[40] K. Heister, M. Zharnikov, M. Grunze, *J. Phys. Chem. B* **2001**, *105*, 4058–4061.
[41] B. T. Meshesha, N. Barrabes, F. Medina, J. E. Sueiras, Proceedings of the 1st WSEAS International Conference on Nanotechnology '09, World Scientific and Engineering Academy and Society, Stevens Point, WI, USA, 2009
[42] P. Villars, K. Cenzual, J. L. C. Daams, F. Hulliger, T. B. Massalski, H. Okamoto, K. Osaki, A. Prince, Pauling File Binaries Edition, Version 1.0, Release 2002/1, ASM International, **2002**.
[43] Q. Jiang, L. H. Liang, D. S. Zhao, *J Phys Chem. B* **2001**, 105–6275.
[44] C. Solliard, M. Flueli, *Surf. Sci.* **1985**, 156–487.